Available online at www.sciencedirect.com

SCIENCE DIRECT

Powder Technology 146 (2004) 121–136

POWDER TECHNOLOGY

www.elsevier.com/locate/powtec

Numerical simulation of Mechanofusion system

Wenliang Chen[a], Rajesh N. Dave[a,*], Robert Pfeffer[a], Otis Walton[b]

[a]*New Jersey Center for Engineered Particulates, New Jersey Institute of Technology, University Heights, Newark, NJ 07102 United States*
[b]*Grainflow Dynamics, 1141 Catalina Dr., PMB-270, Livermore, CA 94550, United States*

Received 7 October 2003; received in revised form 13 July 2004; accepted 13 July 2004
Available online 21 September 2004

Abstract

A numerical simulation of the Mechanofusion (MF) device, which is used for powder surface modification (dry particle coating, mixing, etc.), is carried out using the discrete element modeling (DEM) technique. An existing, widely used, cohesionless contact model (Walton–Braun) is used for two-dimensional simulation studies, in which the particles are assumed to be frictional, elastic-plastic spheres. The Mechanofusion device consists of a rotating cylindrical chamber in which a fixed, eccentrically located, rounded inner-piece and a fixed scraper blade are placed. Two simplified geometric models of the Mechanofusion chamber, one with and the other without the scraper, are studied. Qualitative visualization of the particulate patterns and quantitative diagnostic analysis in the terms of average kinetic energy, rotational energy and collisional granular pressure within two systems demonstrate the effect of the scraper on the particles. The force on the fixed rounded inner-piece, which forms a compression region with chamber wall by its cylindrical surface end, as a function of the rotational speed of the chamber and particle loading is calculated. The numerical simulation results are verified by comparing them with available experimental results. Simulations are also performed to compute useful quantities such as impact forces and collision velocities experienced by the particles due to the interactions with other particles as well as with the vessel walls, and the frequency of collisions within various regions of the device. These quantities are useful for developing a full-scale system simulation that captures the phenomena at multiple length scales.

Keywords: Dry particle coating; Mechanofusion; Discrete element simulations; Soft-sphere modeling

1. Introduction

The Mechanofusion (abbreviated as MF) system was developed in Japan in the mid-1980s and is based on using a high-powered mechanical energy device to dry coat powders without using any liquids [1]. In a dry coating process, tiny, submicron or nanosized (guest or fine) particles are coated onto relatively larger, micron-sized (host or core) particles in order to create value-added composite particulate materials. In contrast to wet-particle coating, the guest particles are brought into close contact with the host particles through the application of mechanical forces. In the past two decades, considerable experimental research and development work has been done in this area, and a number of interesting applications have been proposed and new commercial processes and products have been developed in Japan as well as in the USA (see Ref. [2] for a recent review).

For example, Yokoyama [3] investigated the combination of more than 100 different host and guest particles by the MF process. Tanno [4] reviewed the MF process for producing composite particles. Fig. 1 shows a schematic diagram of the MF system. It consists of a rotating cylindrical chamber in which a fixed rounded inner-piece and a fixed scraper blade are placed. The radius of the inner-piece is smaller than that of the chamber and the clearance space between the inner-piece and the chamber inner wall is adjustable, which generally ranges from 2 to 5 mm. The clearance between the scraper blade and chamber inner wall is much smaller, usually around 0.5 mm. These clearances

* Corresponding author.
E-mail address: rajesh.n.dave@njit.edu (R.N. Dave).

0032-5910/$ - see front matter © 2004 Elsevier B.V. All rights reserved.
doi:10.1016/j.powtec.2004.07.014

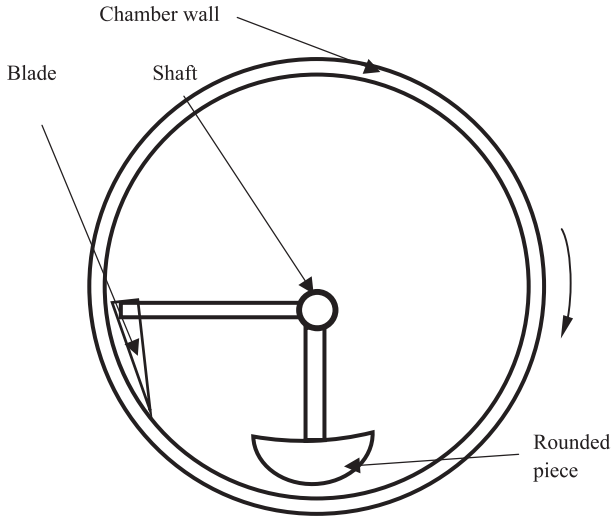

Fig. 1. Schematic diagram of the Mechanofusion system.

are adjustable, and are determined by many factors such as powder properties, particle size, the desired properties of the final coated products, and so on. The powder mixture is deposited inside the chamber for processing one batch at a time.

The operation of the MF process is simple, but the mechanism of powder processing within the chamber is very complicated. When the chamber rotates, powder is forced to the chamber wall by centrifugal action. While passing through the converging space between the rounded inner-piece and chamber wall, mechanical interactions, mainly in the form of high shear-rate collisions, take place between the particles and between the particles and the solid boundaries of the chamber inner wall and the inner-piece. As the particles come out of the diverging space of the inner-piece region, they adhere to each other and to the chamber wall. The blade serves to scrape off the powder attached to the chamber wall. The sheared powder mixture is then re-dispersed into the chamber and moves towards the inner-piece region again. The powder continuously undergoes this process of compression, deagglomeration, and frictional shearing while the chamber is rotating. Since the chamber rotates at high speeds, the interactions are intense and a considerable amount of thermomechanical energy may be generated, which could result in various effects on powder materials.

Various operating parameters, such as the local temperature and the running time are controlled and monitored to prevent thermal degradation of particles.

A number of experimental studies [5,6] have been devoted towards research and development of the MF system. However, there has been very little effort devoted to the theoretical analysis of the Mechanofusion system. One example is the work reported by Chen and Huang [7], in which a preliminary theoretical model of the MF system was proposed to develop quantitative relationships among system variables and their effects. In this model, all of the outcomes of the MF process were assumed to take place in the converging region between the inner-piece and the chamber wall, and this region was referred to as the inner-piece "action zone". The particles within the action zone were treated as a fluid-like assembly. The particle interactions with the inner-piece and the chamber wall were considered; however, the interactions among the particles were neglected. Moreover, the function of the scraper was completely ignored.

The challenge in modeling dry particle coating processes arises from two major factors. First, there is a large difference between the size of the host and guest particles, in most cases, ranging from one to two orders of magnitude. This, coupled with the difference in scale between the device and the host particles, clearly makes a full simulation a multi-scale problem, with three distinct length scales: the device level, the host particle level, and, the guest particle level. Second, there is the problem of the complex geometry of the device and the nature of the motions and forces within the system, including the effect of air or other fluids present. Overall, the modeling should take into account the mechanism of the motion of the device and the nature of collisions, i.e., intensity and frequency of collisions among particles and between the particles and the device. It should also account for the agglomerate break-up and transfer of guest particles from one host particle to another. A successful long-term research plan would have to take into account all of these aspects by dividing them into subparts, and in this way, a reasonable understanding of the dry coating process can be obtained.

In a coating application, the actual volume of the guest particles (about 0.1% to 2% by weight of the host particles) is very small; however, the number of guest particles is extremely large. Due to the computational limitations, it is impractical to include the fine particles in this modeling effort. The main purpose of this work is to compute useful information based on host/host and host/boundary interactions, including an analysis of the kinematics and dynamics of particle collisions, such as the frequency of collisions and their strength, for developing a basis for a full-scale system simulation that may capture the phenomena at multiple length scales. It is believed that the effect of the presence of the fine guest particles may, in future work, be included in terms of change in certain properties of the host particles. Thus, the objective of this paper is to perform numerical simulations of the Mechanofusion system with a monodisperse system of host particles using the Discrete Element Method (DEM), originally proposed by Cundall and Strack [8].

In setting up the numerical model, realistic interparticle force models are considered for investigating the interaction of each host particle with other particles, the boundaries (chamber and inner-piece), as well as the blade (scraper). First, a diagnostic analysis is carried out to compare two systems, one with a scraper and one without. This is done to examine the effect of the scraper, and to determine if

ignoring the scraper in modeling, as was done by Chen and Huang [7], is valid. Next, in order to validate the numerical model against the experimental results, the force on the inner-piece is calculated at various operating conditions to compare with available experimental results. After gaining confidence in the numerical model, a number of simulations are performed, including detailed computations of quantities such as average forces on host particles categorized by various functional zones within the chamber. Finally, collision analysis is performed based on particle–particle and particle–boundary interactions aimed at understanding the various mechanisms occurring within the system.

2. Description of the model

2.1. Geometric model

In the model, as shown in Fig. 2, the outer circle represents the Mechanofusion chamber and the eccentric inner circle represents the rounded inner-piece. Exact modeling of the scraper is very complicated; therefore, only the main function of the scraper, which is to provide an obstruction, that diverts particles from the outer wall, is modeled in the simulations. Here we have represented the scraper by a set of fixed particles placed at an angle as shown in the inset of Fig. 2. This closely mimics the actual placement of the scraper within the chamber. In the numerical model, we assume zero clearance between the scraper particles and the chamber (without any interaction between scraper and the chamber). These fixed particles are taken to be of the same size as the host powder particles.

2.2. Force model

For the normal force, a partially latching-spring model proposed by Walton and Braun [9] for an elastic-plastic material is adopted in this study. In this model, the loading resistance force is a linear spring, with the spring constant given by K_1. A stiffer linear spring is used during the unloading (restoration) stage, with spring constant K_2, while a finite plastic deformation occurs. K_2 can be obtained from the coefficient of restitution e, assumed to be independent of the impact velocity for the elastic-plastic case considered here, and is defined as

$$e = \sqrt{\frac{K_1}{K_2}} \tag{1}$$

The normal force is given by

$$\begin{cases} N_{\mathrm{l}} = K_1\alpha & \text{for loading} \\ N_{\mathrm{u}} = K_2(\alpha - \alpha_0) & \text{for unloading} \end{cases} \tag{2}$$

where α is the relative approach (overlap) after initial contact, and α_0 is the finite plastic deformation, i.e., α_0 is the value of α when the unloading curve goes to zero.

The tangential force model used here is the incrementally slipping friction model, also proposed by Walton and Braun [9]. The effective tangential stiffness, K_{T} is given by

$$K_{\mathrm{T}} = \begin{cases} K_0\left(1 - \frac{T - T^*}{\mu N - T^*}\right)^{\gamma} & \text{for slip in one direction } (T \text{ increases}) \\ K_0\left(1 - \frac{T^* - T}{\mu N + T^*}\right)^{\gamma} & \text{for slip in another direction } (T \text{ decreases}) \end{cases} \tag{3}$$

where N is the total normal force, and T is the total tangential force; K_0 is the initial tangential stiffness, which can be calculated from normal stiffness by the equation $K_0=\tau K_1$ for loading and $K_0=\tau K_2$ for unloading, and τ is less than 1.0; μ is the coefficient of friction, and γ is the exponent, which is set to one for all cases in this paper; T^* is the loading reversal value, which is initially zero, but it is subsequently set to the value of the total tangential force T whenever the relative tangential slip reverses direction. It is scaled in proportion to any change in the normal force from the previous time step.

The new tangential force T' is given by the expression

$$T' = T + K_{\mathrm{T}}\Delta S \tag{4}$$

where ΔS is the amount of relative surface displacement between the contact particles.

Thus, in order to calculate the total tangential force acting between each pair of particles, one needs to keep only two history dependent quantities, T and T^* from one time step to the next, minimizing the complexity of the data-structure used in computations.

The calculation time step is related with normal stiffness K_1 by the equation, $\Delta t = \frac{\pi e\sqrt{m/2K_1}}{n}$, where m is mass of the particle and e is the coefficient of restitution. In our simulation, the calculation time steps n for each contact is taken to be 40. A larger stiffness results in smaller time steps and longer computation times. On the other hand, a smaller stiffness value allows a larger time step and a shorter computation time. However, unduly small stiffness causes a time step with unstable simulation results. We have observed that under stable conditions, the value of stiffness does not significantly change the kinematics of the results, as long as significant overlap does not occur during collisions. This fact has also been shown in previous

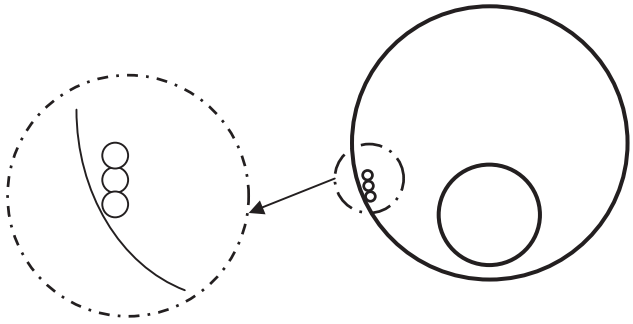

Fig. 2. Simulation model of the Mechanofusion system where the scraper is modeled as several fixed small particles and the inner-piece is a large fixed particle.

simulations of rapidly flowing granular systems [10,11]. It is noted that using small value of stiffness will provide inaccurate results for the contact forces. The significance and magnitude of the error in the force calculations will be explored in a subsequent paper.

2.3. Simulation approach

In a dynamic simulation such as this, the computation time is a critical issue. The number of particles should be large for the simulation to capture the essential features of the particulate flow system. However, the number of particles dictates the computation time, and hence the computational cost and the user's waiting time. The CPU time increases as $n\log(n)$ where n is the number of particles. One way to limit the number of particles in the system is by using a two-dimensional approximation for the system. Dimensional reduction is equivalent to assuming the system having an infinite length in the third (eliminated) dimension or that the interaction along this dimension could be neglected. In the former case, the flow pattern becomes independent of the third direction [12]. Approximation for the latter case becomes possible as the particulate flow becomes predominantly two-dimensional.

In a Mechanofusion system, the interactions of a particle with other particles and the system boundary can be considered in a transverse x–y plane and the particulate flow can be approximately treated in the plane. The transport of the particle in the third dimension (z-direction) does not play an import role in the system. Therefore, we can justify using a two-dimensional system to simplify the simulation. However, a limited number of test cases were run in 3-D, with periodic end conditions as well as with stationary end walls having a cell thickness of 10 particle diameters, to validate the results of 2-D simulations. These 2-D/3-D comparisons are shown in Section 3.1.3, indicating that 2-D simulations are adequate for the purpose of gaining a basic understanding of the system. The parameters used for the simulation system are given in Table 1. Unless specified otherwise, those values are applied to the rest of simulation work. It is noted that the simulated system is much smaller than the actual physical system so that fewer particles can be used, while still preserving the overall loading of the chamber. The normal stiffness K_1 is selected according to impact mechanics and the condition that the maximum particle deformation is less than 1%. As already mentioned, previous simulations have demonstrated [10] that for rapidly flowing granular systems, the kinematics of the flow are insensitive to the exact value of the normal stiffness as long as it is sufficiently large to prevent significant overlaps. The objective of the current paper is to examine the kinematics of the system; hence, the selection of the stiffness is not expected to have a significant impact on the results of interest. The rest of input parameters are selected based on expected empirical values. Different values, for example, of the coefficient of friction might have a quantitative effect on the simulation results; however, the qualitative phenomena are captured by using a reasonable set of values. We plan to include a systematic parametric investigation in a future paper.

Table 1
Typical parameters for the simulation system

Radius of particles	0.2 mm
Number of particles	1500
Density of particles	1.20×10^3 kg/m^3
Diameter of chamber	25 mm
Diameter of inner cylinder	10 mm
Diameter of scraper	0.4 mm
Gap of cylinders	0.8–1.6 mm
Rotational speed of chamber	1000–4000 rpm
Normal stiffness (for loading)	20,000 N/m
Particle–particle coefficient of friction	0.4
Particle–solid boundaries coefficient of friction	0.5
Coefficient of restitution	0.85

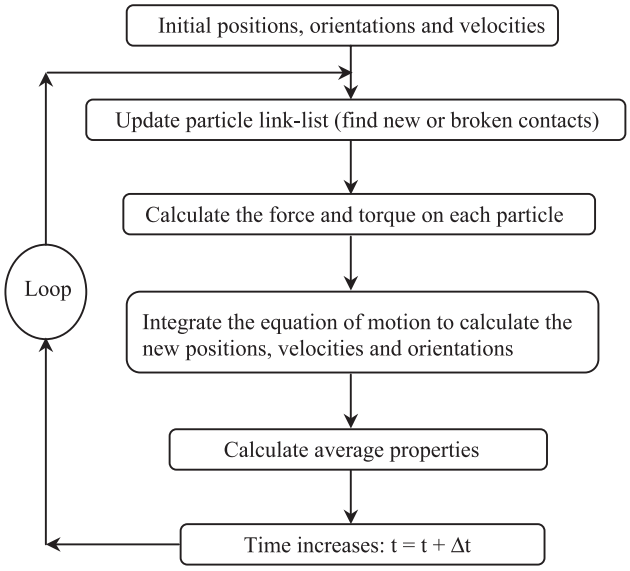

Fig. 3. Algorithm of DEM simulation.

2.4. Numerical method

As described in the geometric model, during simulation, two cylinders (chamber and inner-piece) are treated as boundary particles and the scraper is represented as fixed particles. They act as discrete elements of the system, which interact with the particles in motion. The computational algorithm for the soft sphere model utilized here is illustrated in Fig. 3. At the beginning of the simulation, particles are randomly positioned inside the system. Initially, particles are also assigned small random velocities; however, the net momentum of the system is initially zero. For each time step, interparticle forces are calculated for all contacting particles using the force model. Since the simulation is implemented in a 2-D mode in this study, the gravity force, which is in z-direction, is not considered.

Summation of the forces acting on each particle is carried out in x and y directions, respectively. The new translational and rotational accelerations of the particle are calculated by Newton's equation of motion (shown here for the x-direction)

$$\begin{cases} \dot{v}_x^n = \frac{F_x^n}{m} \\ \dot{\omega}_x^n = \frac{M_x^n}{I} \end{cases} \tag{5}$$

where the superscript n refers to the current time step, m=1/6 $\pi d^3 \rho$ is the particle mass, d is the particle diameter, and ρ is the particle density; I=1/10 md^2 is the particle moment of inertia, and F_x and M_x are the interparticle force and moment acting on the particle due to interaction with others. Similar equation can be written for the y-direction.

The moment of inertia defined above is for a sphere restricted to a plane, and not for a disk-shaped particle. Thus all spheres are restricted to a plane in 2-D motion. The new velocity and position of the particle are obtained by explicit integration of Newton's equation via the time-centered, finite-difference "leap-frog" method [13]. The finite difference equations for the particle are

$$\begin{cases} v_x^{n+\frac{1}{2}} = v_x^{n-\frac{1}{2}} + \dot{v}_x^n \Delta t \\ \omega_x^{n+\frac{1}{2}} = \omega_x^{n-\frac{1}{2}} + \dot{\omega}_x^n \Delta t \end{cases} \tag{6}$$

for translational and rotational velocity in the x-direction. The new particle position is updated by

$$x^{n+1} = x^n + v_x^{n+\frac{1}{2}} \Delta t \tag{7}$$

for the x-direction and similarly, corresponding equations for motion can be written for the y-direction. After obtaining new positions and velocities for all the particles, the program repeats the cycle of updating contact forces and particle positions. Checks are incorporated to find new contacts and delete broken contacts for the neighbor list of each particle. During simulation, average properties of the system are calculated and are written to a file at regular intervals to obtain quantities of interest.

2.5. Computing diagnostic quantities

The quantities of interest for diagnostic analysis of the simulated system are the time-averaged values of the collisional granular pressure, velocity, rotational kinetic energy, and so on. The time over which averages are taken must be long enough compared to the typical time taken by any particle interaction (e.g., particle–particle or particle–wall collision), but it should be short compared to the time scale of major changes in the properties of interest.

In the numerical simulation, first, two different geometric models of the MF systems are studied. The two models differ only in that the scraper is excluded in one of the models. The function of the scraper is primarily to scrape off the particles caked on the chamber surface after passing through the compression region, which is formed by the gap between the inner-piece and chamber wall. For the purpose of averaging the quantities of interest, the whole region is divided into a series of equal-volume annular zones (i.e., the volume of each zone is V_i=V/N, where V is the volume of the chamber and N is the number of zones). The number of zones is selected so that the radial width of each zone is equal or greater than the maximum diameter of particles. Therefore, the largest particle cannot occupy more than two zones at a given time instant. The simulated region is divided into seven zones, as shown in Fig. 4; note that the figure is not to scale. In addition to the annular zoning, a second partitioning of the space into regions, varying in the circumferential direction, was also done to highlight the differences between the systems with and without the scraper. This partitioning, and the results are described later.

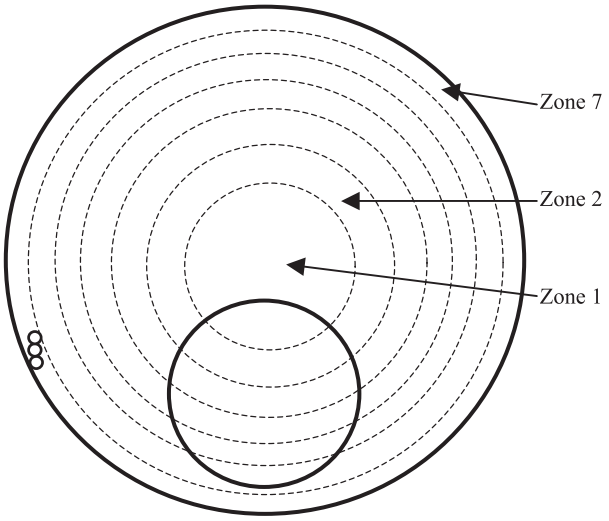

Fig. 4. The Mechanofusion system is divided in seven equal volume zones (not to scale).

3. Simulation results

3.1. Comparative diagnostic studies of the Mechanofusion system with and without the scraper

The purpose of this comparative study is to understand the effect of the scraper on the dynamics of the system. The number of particles is 1500 and the gap between the inner-piece and the chamber boundary is 1.6 mm. The rotational speed of the chamber is 2000 rpm, and the total operation time is 10 s, which is found to be adequate for capturing steady-state behavior.

Figs. 5a and 6a show snapshots of the particle patterns within the system with the scraper and without scraper, respectively. The initial condition for the two systems is the same: the particles are randomly placed in the chamber with a small initial velocity. From these figures, the time evolution of the particle patterns can be observed. Fig. 5a shows the sequence (at 2-s intervals) of the particle patterns

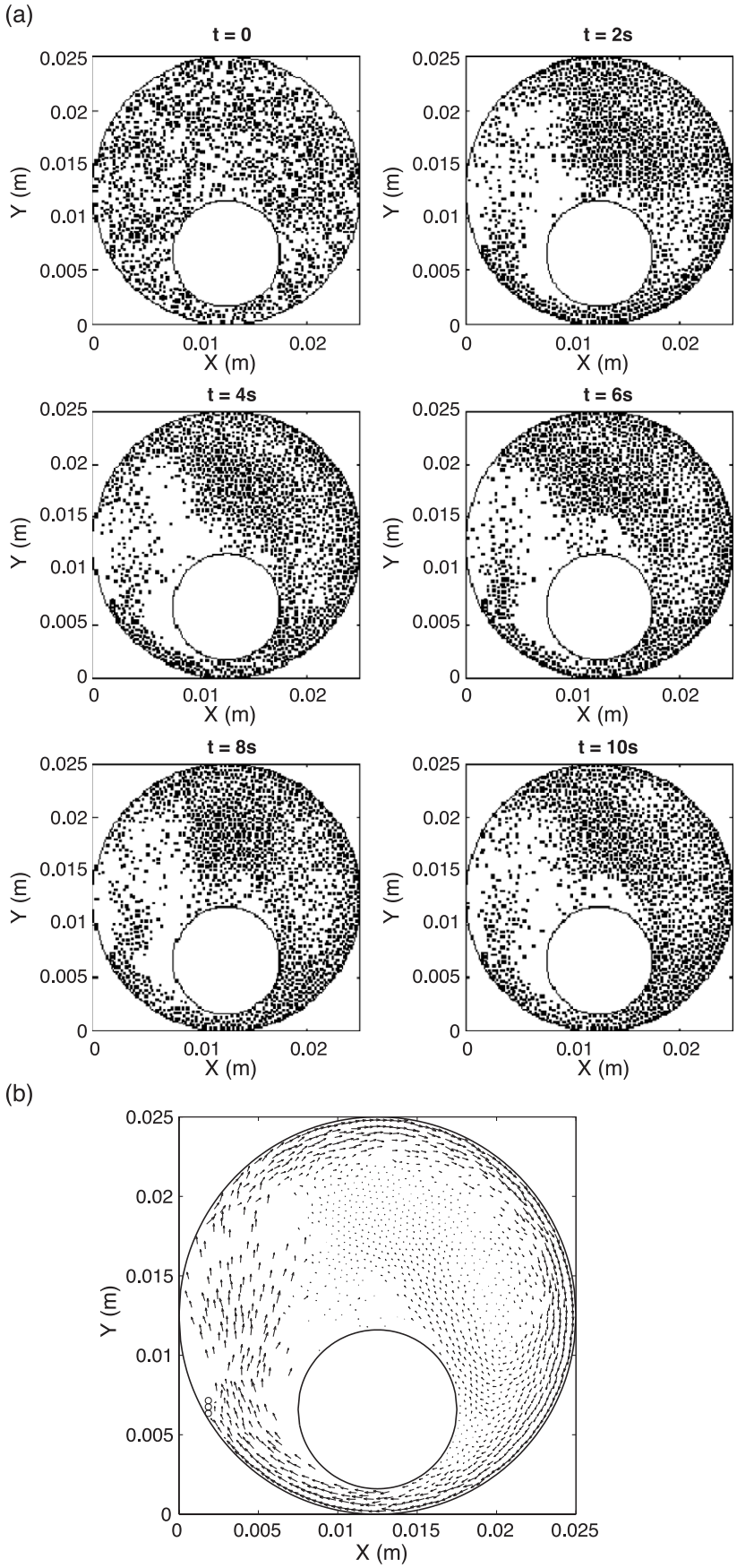

Fig. 5. A sequence of snapshots of the system with scraper showing (a) the particle pattern from 0 to 10 s, and (b) the velocity vectors at 2 s.

for the system with a scraper. It can be seen that during the operation particles are well dispersed within the chamber, and within the first 2 s, the system is close to steady state. However, the sequence of the particle patterns shown in Fig. 6a for the system without a scraper is quite different from that shown in Fig. 5a. As time passes, more and more particles get attached to the chamber wall because of the centrifugal force, and hence the particles are not uniformly dispersed within the system.

Corresponding snapshots of velocity vectors at time 2 s are shown in Figs. 5b and 6b, respectively. These vector plots indicate even more clearly how the particle motion differs in the two systems. As can be seen, for the system with a scraper, there are zones of swirls and chaotic motion, while for the system without a scraper, the particles essentially move in a tangential direction along the outer wall of the chamber, and the motion of the particles in the rest of the chamber is negligible. Hence, it appears that the scraper provides a great deal of agitation to the particles.

The snapshots of the particle patterns within these two systems show only a qualitative difference between the system with and without the scraper. To obtain a quantitative understanding, the time-averaged kinetic energy, pressure, etc., can be computed. These computations provide insight into the dynamics of the system. Hence, a diagnostic analysis is carried out to compare the difference in the dynamic conditions within the two systems. Each diagnostic quantity is volume-averaged for each zone during a time period set equal to 2 s, after the system attains steady state. Since the simulation is in 2-D, the volume is obtained by setting the third dimension, i.e., the thickness of each zone, to be equal to the diameter of a particle.

3.1.1. The rotational kinetic energy

The rotational kinetic energy in each zone is computed from the following equation

$$E_{\mathrm{r}}^{(k)} = \frac{1}{2V_k} \sum_{i \in k} I_i \left[\omega_{ix}^2 + \omega_{iy}^2 + (\omega_{iz} - \omega)^2 \right] \tag{8}$$

where V_k is the volume of the zone k, ω is the rotational speed of the MF chamber, and ω_{ix}, ω_{iy}, ω_{iz} are the components of the angular velocity of the particle i; I_i=2/5 $m_i r_i^2$ is moment of inertia of the particle, and m_i and r_i are the mass and radius of the particle. For a two-dimensional simulation, ω_{ix}=ω_{iy}=0. In the above equation, the rotation speed of the chamber is subtracted so that the effect of the rigid body rotation is eliminated. For instance, if all the particles were glued to the chamber, the rotational kinetic energy of each particle would be $I_i\omega^2$ and the computed total rotational kinetic energy from Eq. (8) would be zero.

Since the particles attain steady-state conditions in less than 2 s, the rotational kinetic energy of the particles is plotted in Fig. 7, averaged over the time period from 2 to 4 s. For the system with a scraper, Fig. 7a, the rotational kinetic energy increases along the radius, which means that the boundary zones have larger rotational kinetic energy. However, for the system without a scraper, Fig. 7b, the rotational kinetic energy along the boundary zones is significantly lower. This implies that without the scraper, particles stick to the boundary during the processing, and undergo mostly rigid body rotation.

3.1.2. The translational kinetic energy

The deviatoric translational kinetic energy is calculated by

$$E_{\mathrm{t}}^{(k)} = \frac{1}{2V_k} \sum_{i \in k} m_i [(v_i - \bar{v}_k)^2] \tag{9}$$

where v_i is the particle velocity and $\bar{v}_k$ is the average velocity computed based on the average velocity field at the location of particle i. Our averaging zones were not fine enough to generate an accurate 'average velocity field' defined at each point inside the simulated chamber. As a consequence, in order to compare the relative kinetic energy of particles in each system, we used an approximate kinetic intensity indicator for each zone based on the differences of the value of the particle's velocity in the radial, tangential and vertical direction (i.e., in cylindrical coordinates) and the corresponding average value of the particle velocities in the zone,

$$E_{\mathrm{t}}^{(k)} = \frac{1}{2V_k} \sum_{i \in k} m_i \left[(v_{r_i} - \bar{v}_{r_k})^2 + (v_{\theta_i} - \bar{v}_{\theta_k})^2 + (v_{z_i} - \bar{v}_{z_k})^2 \right] \tag{10}$$

where v_{r_i}, v_{θ_i}, v_{z_i} are the particle velocities in the radial, tangential and vertical direction, and $\bar{v}_{r_k}$, $\bar{v}_{\theta_k}$, $\bar{v}_{z_k}$ are the average velocities for zone k where particle i appears in the current time step, respectively. In a 2-D system, velocity in the vertical direction (z-direction) v_{z_i}=0. This approximate kinetic intensity indicator provides an indication of which annular regions have high deviatoric velocities (although it is not an accurate measure of the true deviatoric kinetic energy, nor of the granular temperature).

Fig. 8 shows the kinetic intensity indicator distribution within the chamber for the systems with and without the scraper. Fig. 8a shows that for the system with a scraper, the kinetic intensity is nearly evenly distributed within zones 3 through 7, i.e., the outer half of the chamber. However, for the system without a scraper, Fig. 8b, the kinetic intensity is much smaller compared with the value for the system with scraper, and is significant only in zone 6, where most of the collisions between the particles and the rounded inner-piece take place. Generally, the average value within the system with the scraper is more than twice as that for the system without the scraper.

3.1.3. The granular pressure

For a particle dynamic system such as MF, the granular pressure can be estimated based on the work by Ladd [14],

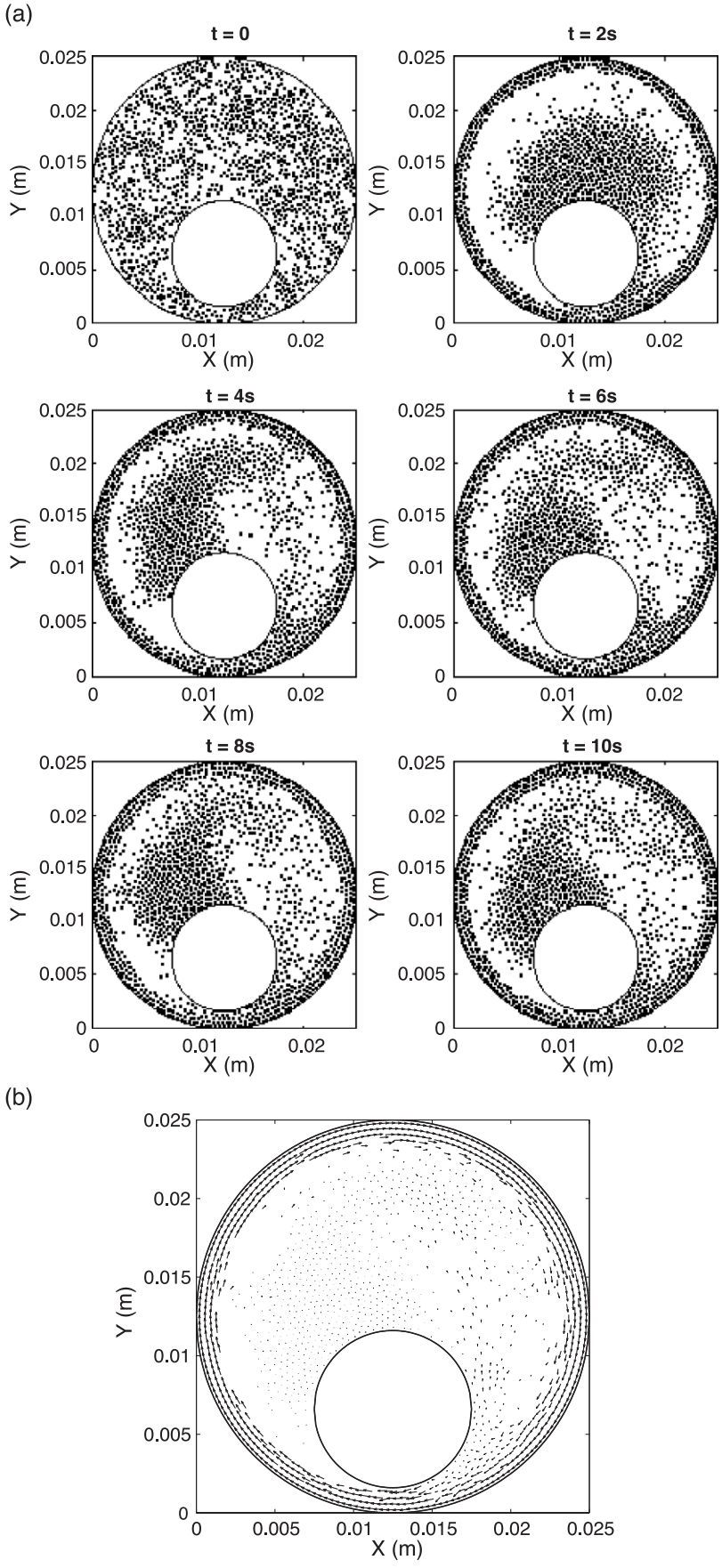

Fig. 6. A sequence of snapshots of the system without scraper showing (a) the particle pattern from 0 to 10 s, and (b) the velocity vectors at 2 s.

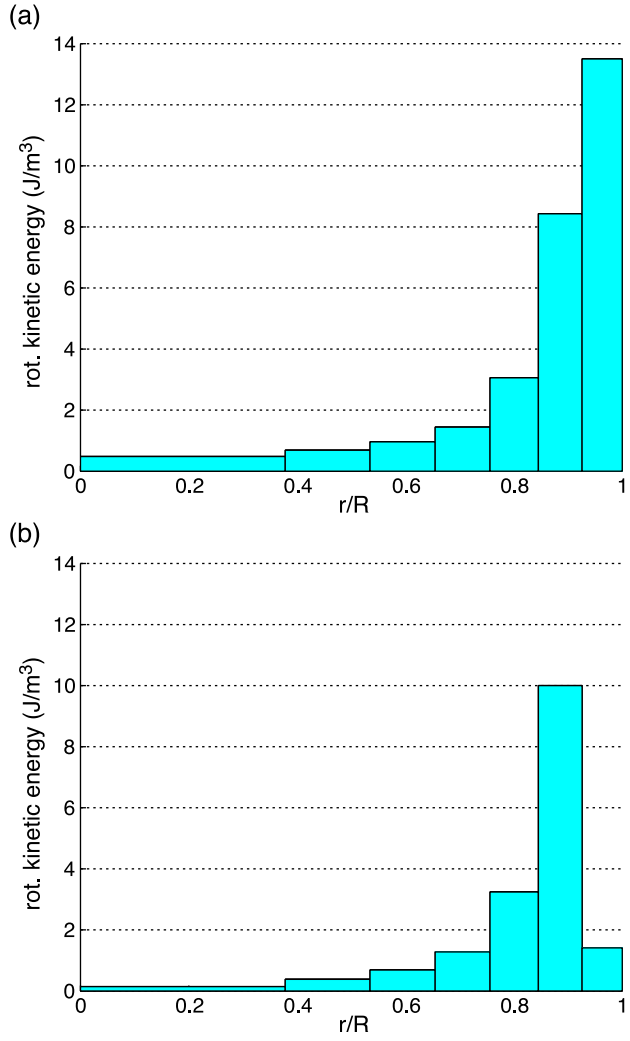

Fig. 7. Rotational kinetic energy distribution in the Mechanofusion chamber averaged between 2 and 4 s for (a) the system with scraper and (b) the system without scraper.

and is also described by Walton [15,16]. The equation is given by

$$P = \frac{1}{3V_i}\left[\sum_{i\in k} m_i(v_i - \bar{v}_k)^2 + \sum_{i\in k, i>j} F_{ij}R_{ij}\right] \quad (11)$$

where F_{ij} is the repulsive force acting between particle i and j, and R_{ij} is the distance between particle i and particle j. The first term in the above expression is the kinetic contribution to the granular pressure due to the motion of the particles corresponding to the deviatoric velocity computed based on the average velocity field at the location of particle i, and the second term is the potential or collisional contribution to the granular pressure, which is due to the interaction forces between the particles. While the granular temperature and the kinetic part of the granular pressure are important from the point of view of kinetic theory analyses, they only indirectly contribute to collisions. They are also quantities that require more precise descriptions of the mean velocity field than we had in our simulations. In studying the functional operation of the Mechanofusion system, we are primarily concerned with the effects of collisions, collisional stresses and momentum transfer among particles and between particles and walls. Thus we concentrate on evaluating the second term in Eq. (11), the collisional or contact contribution to the granular pressure in various regions inside the simulated MF device.

The collisional pressure distribution for the systems with and without the scraper is shown in Fig. 9a and b, respectively. It can be seen in the figure that the collisional/contact pressure along the boundary zone (zone 7) is very large compared with the other zones. The value for the boundary zone of the system without the scraper is relatively larger due to a large number of particles in that zone, densely packed against each other along the boundary. In comparison, the collisional/contact pressure distribution for the system with the scraper is lower, although somewhat more uniform along zones 5 and 6. Overall, the average collisional pressure for the entire region for the system

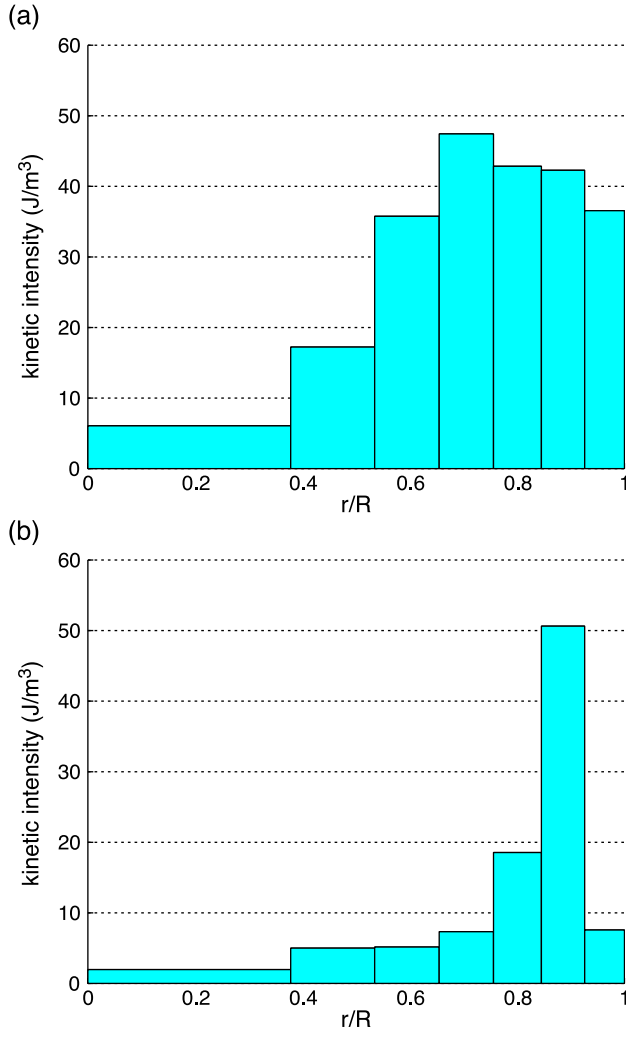

Fig. 8. Kinetic intensity distribution in the Mechanofusion chamber averaged between 2 and 4 s for (a) the system with scraper and (b) the system without scraper.

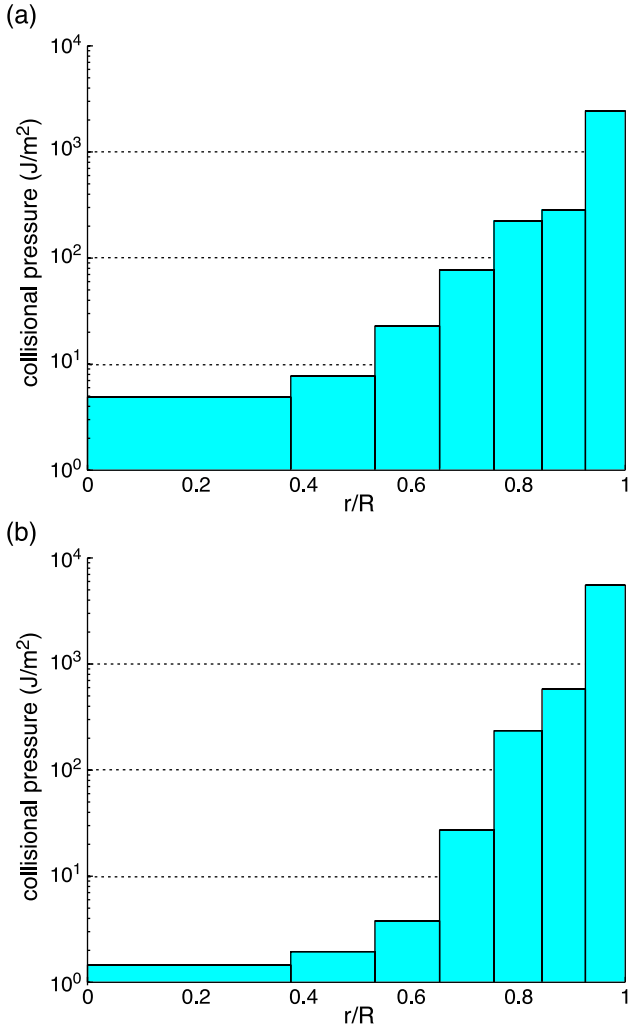

Fig. 9. Collisional pressure distribution inside the Mechanofusion chamber averaged between 2 and 4 s for (a) the system with scraper and (b) the system without scraper.

without the scraper is nearly twice that of the system with the scraper primarily because of the contribution from the particles in nearly continuous contact near the outer wall.

The overall results for quantities such as the kinetic intensity and collisional granular pressure are not significantly different if the simulated system is 3-D instead of 2-D, which is verified by simulating in 3-D in two ways. First, we examine a 3-D system with periodic boundaries in the z-direction and having a cell thickness of 10 particle diameters; and second, the system having rigid walls on both ends, with separation between them of 10 particle diameters. The results of averaged values for the kinetic intensity factor and collisional pressure as a function of time for both the 2-D and 3-D systems are illustrated in Fig. 10a and b, respectively. As can be seen, the value of the average kinetic intensity in the 2-D system is very close to the value in the 3-D system with periodic boundaries, whereas it is larger than the value in the 3-D system with rigid walls in the z-direction, which confine the movements of particles in this direction. On the other hand, the average collisional pressure is larger in the 3-D system with bounded walls than the other two systems, because of the interactions of particles with boundary walls. Generally, the differences are not more than about 10%, indicating that the 2-D simulations are adequate for revealing important phenomena regarding the flow kinematics.

The comparative diagnostic study of the MF system shows that the numerical simulation can provide detailed information about the flow patterns and dynamics of the system. A comparison of the system with and without the scraper clearly shows the important role played by the scraper, suggesting that the scraper does much more than simply eliminate caking of the powder; it also significantly improves the dispersion of powder within the system.

3.2. Dynamics of collisions in the Mechanofusion system

In this section, a force analysis designed to aid in understanding the interactions within the MF system at the microscale is described. First, the force on the inner-piece as a function of the rotational speed of the chamber, as well as the loading of the system is calculated and compared with the experimental results reported by Yokoyama et al. [3]. This is a diagnostic quantity that can actually be measured experimentally, and can be used to monitor the system during its operation, and for analyzing power-consumption. A comparison of the experimental and numerical results can provide the validation of the computer modeling utilized in this paper. This is followed by a calculation of the average forces on each particle, categorized by several important areas within the system. When not specified, the particle loading is 1500 particles and the gap size of the inner-piece is 1.6 mm.

3.2.1. Forces exerted on the inner-piece

The methodology of the DEM soft sphere technique makes it possible to keep track of all the interactions of the particles with the inner-piece at any instant of time. Therefore, the force on the inner-piece is calculated as a long-term averaged value, obtained by averaging all the instantaneous values during the simulation. Both the normal force and tangential force are calculated.

First, the forces on the inner-piece as a function of the rotational speed of the chamber are computed, and are shown in Fig. 11a. In this figure, the points represent simulation results. It is observed that the calculated normal and tangential forces on the inner-piece increase linearly with the rotational speed of the chamber on a log–log plot. A trend line is also plotted as shown, with a power-law constant of 2, which is very close to the actual best-fit value of 1.97. An experimental study reported by Yokoyama et al. [3] for polystyrene beads as a function of the rotation speed also shows a linear relationship for the normal and tangential forces on a log–log plot. This is shown in Fig. 11b, which is reproduced with permission of the publisher. Also, the ratio of the calculated normal force to the

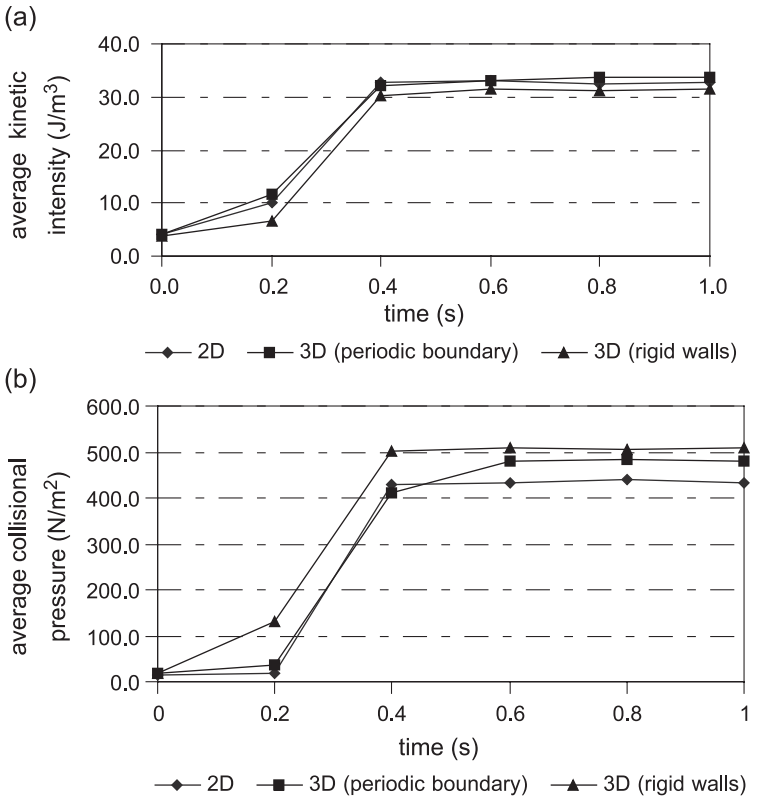

Fig. 10. Averaged results for 2-D and 3-D simulations for the Mechanofusion system with scraper as a function of time, (a) kinetic intensity, and (b) collisional pressure.

tangential force (around 5) is similar to what is found in the experimental results. The 2-D simulations show that both the normal and tangential force on the inner-piece vary as nearly the square of the rotational velocity. The experimental results of Yokoyama indicate that the normal force varies with the rotational speed to approximately the 2.1 power, while the tangential force is not quite a simple power law, but has a slope slightly higher than 2 at low speeds and somewhat less than 2 at higher rotational speeds. Although a systematic sensitivity study has not yet been performed to completely verify the robustness of the simulation results, it is expected that this power-law dependence of the forces on the inner-piece varying with the square of the rotation rate is a robust property of the MF system. This expectation is supported by the fact that no adjustments were made to any of the assumed simulated particle or wall properties in order to obtain this result, and it is highly unlikely that such a good agreement with experiments would have been obtained unless the power-law relationship is relatively insensitive to the choice of specific interparticle or particle–wall interaction parameters.

Next, the normal and tangential forces on the inner-piece are examined as a function of the particle loading in the system. The simulation is carried out under five different loadings: 500, 800, 1000, 1200 and 1500 particles. For each loading, three different values of the rotational speed of the chamber, 1000, 2000 and 3000 rpm are considered. The results of the normal force and tangential force vs. loading and rotating speed of the chamber are shown in Figs. 12 and 13a, respectively. Note that the values of the normal and tangential forces for a loading of 500 particles are quite small, but are nonzero. Both the normal and tangential forces on the inner-piece increase with load. For each rotational speed, the rate of increase of the force gradually decreases with particle loading, which is similar to the behavior observed in the experimental study. The rate of increase is larger for higher rotational speeds of the chamber. The numerical results qualitatively agree with the experimental results shown in Fig. 13b (reproduced with permission from the publisher), and provide further verification that the trends calculated in the numerical simulations are generally consistent with measurements.

3.2.2. Forces on the particles during impact

In the MF process, the particles experience different interactions within the system. The average force that a typical particle experiences is one of the indicators of the overall dynamic performance of the system. The duration of individual collisions and the peak force during a collision is known to be a strong function of the interparticle stiffness (and/or the specific form assumed for the interaction force–displacement relation). The total momentum transferred during a collision, on the other hand, depends on the time-integral of the forces acting during the collision. That time-integral of the force, which controls the kinematics of the flow, is relatively insensitive to the stiffness of the

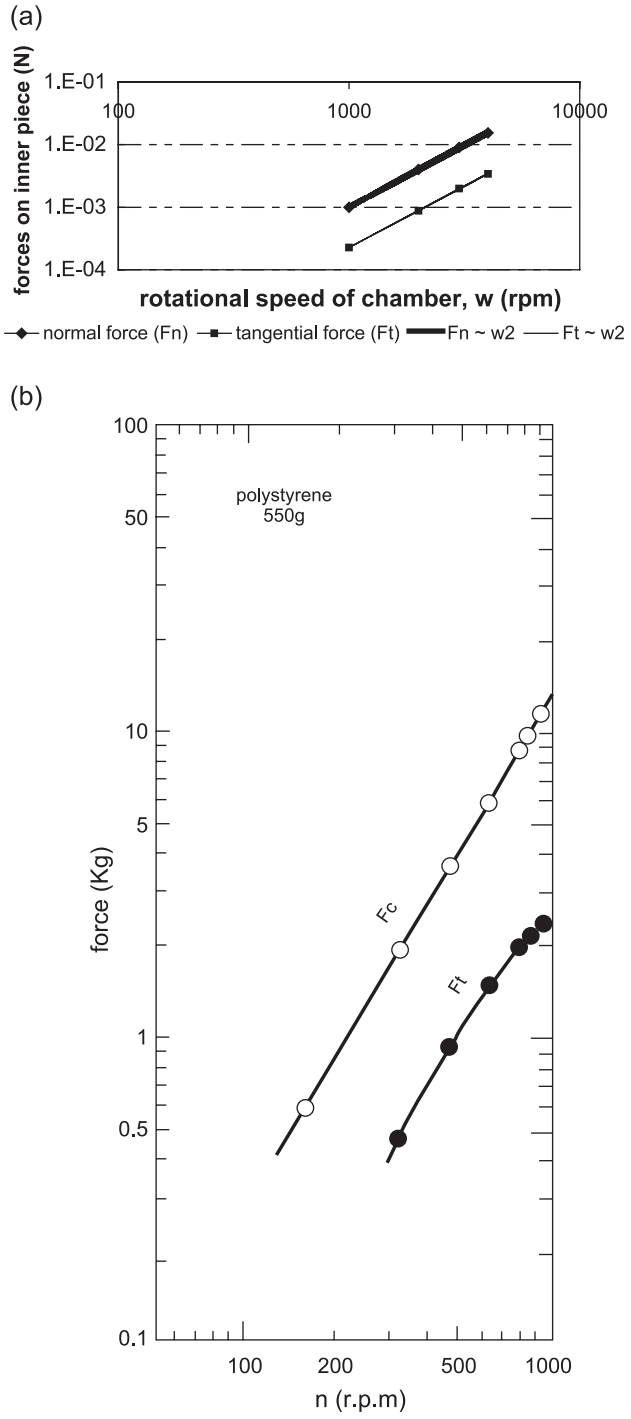

Fig. 11. Average normal and tangential forces on the inner-piece vs. the rotational speed of chamber, (a) simulation results, where the solid lines are trend-lines indicating that the forces are proportional to the square of the rotational speed, (b) experimental results from Yokoyama, KONA, 1987 (reproduced with permission).

interparticle interaction force–displacement relation (e.g., K_1 in Eq. (1)). The time average of the interaction forces experienced by particles in a region is an indication of the average momentum transfer by collisions in that region, and is not strongly sensitive to the specific stiffness chosen for the interparticle interactions. Moreover, within the chamber,

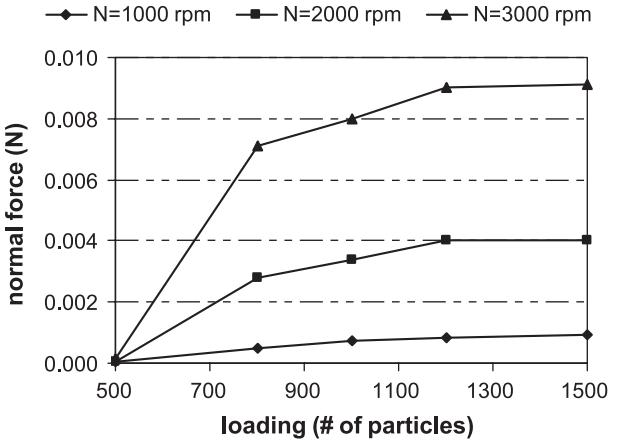

Fig. 12. Average normal force on the inner-piece vs. the loading of particles and the rotational speed of the chamber from simulations.

different areas or zones will show different behavior, as was shown in the previous section. For this and subsequent sections, four new areas, different from the seven zones used before, are defined in Fig. 14. Area 1 is the "inner-piece area", which includes the converging-diverging region; Area 2 is the "scraper area" since the action of the scraper

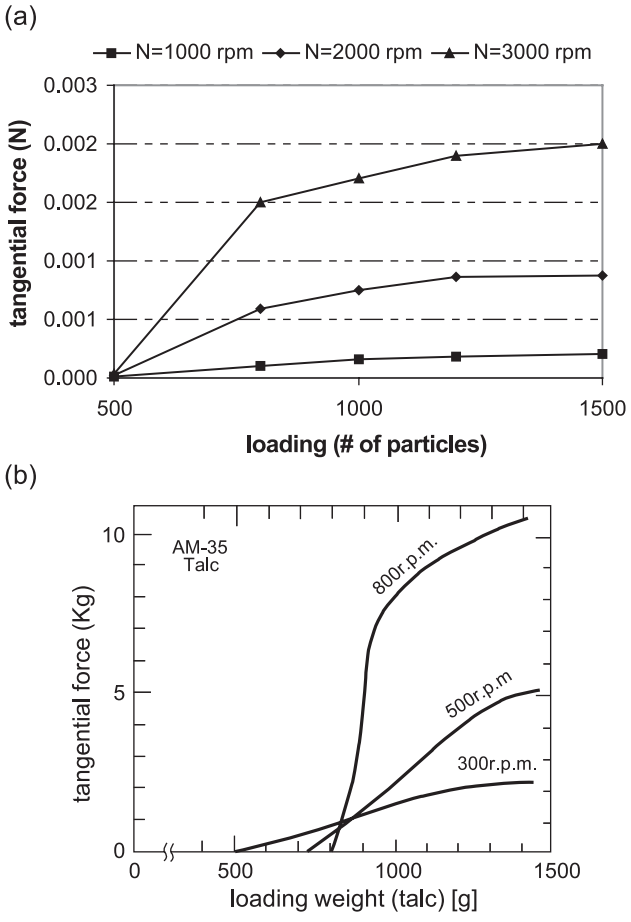

Fig. 13. Average tangential force on the inner-piece vs. the loading of particles and the rotational speed of the chamber, (a) simulation results, (b) experimental results from Yokoyama, [3] (reproduced with permission).

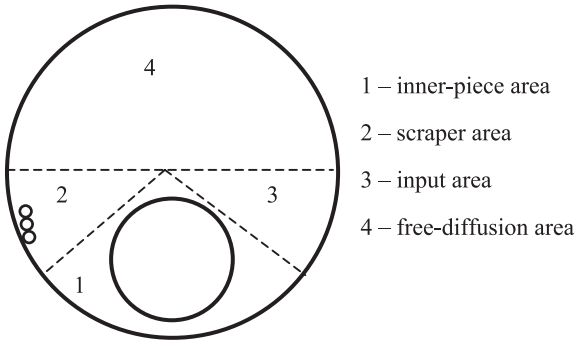

Fig. 14. Definition of four major areas within the Mechanofusion chamber.

dominates this area; Area 3 is the "input area", because it is the area where the particles arrive before they enter the inner-piece area, and Area 4 is the "free-diffusion" area, where particles get freely dispersed after being removed from the wall by the scraper. Various quantities of interest are calculated for each area, such as the average normal and tangential force on a particle during time t=2 to 4 s as shown in Fig. 15. Here the operating parameters are the same as before in the comparative study.

As seen, the average normal force on the particles is about four times larger than the tangential force. That indicates that the MF system produces significant normal forces in addition to shearing forces. As can be expected, the average forces on the particles in the inner-piece and the scraper areas are much larger than the forces in the other two areas. This means that powder coating is more likely to occur mainly within the inner-piece and scraper areas where high collisional momentum transfer is occurring. These plots also show that the time-averaged interparticle forces in the scraper area are slightly larger than those in the inner-piece area, which is somewhat counterintuitive. There are two issues here; first, the time-averaged interparticle forces in the inner-piece area are inversely proportional to the gap size. For this particular simulation system, the gap size of 1.6 mm is somewhat high, and when it is reduced to 1.0 mm, the interparticle forces within the inner-piece area become much larger than in the scraper area. Second, the interparticle collision force is not the only parameter that governs the coating activity. As will be shown later, the frequency of collisions in the inner-piece area is much higher, indicating that significant mechanical work related to coating activity is likely to take place in that region.

In order to keep the number of computations at a reasonable value, the spring-stiffness in the force model is chosen to be much smaller than that of a real particle material. While this choice provides reasonable results for the kinematics of the system, the actual values of the instantaneous computed forces are lower, and the contact durations are higher, than would be expected for real particle–particle collisions (with higher effective stiffnesses). The results shown in this section should therefore be considered primarily as qualitative indications of what is happening within the system. It is, perhaps, more instructive to examine the collision velocities of the particles in the simulations, instead of the collision forces, to get a more accurate picture of the nature of the strength of the collisions. This is done in the next section.

3.2.3. Relative velocities of the particles during impact

In Fig. 16, the relative normal impact velocities for the four different regions as well as average values in the whole system are plotted, with and without the presence of the scraper. As can be seen, the relative normal velocities in the inner-piece and the scraper regions are higher than those in the other two areas. In line with the results of Fig. 15, the scraper area shows values slightly higher than the inner-piece area, but this is reversed (not shown) when the gap size is reduced. When the two systems are compared, it is clear that the average normal impact velocities with the scraper present are twice those without the scraper.

The picture is somewhat different when the relative impact velocities in the tangential directions are computed, as seen in Fig. 17. The system without the scraper has a higher average tangential velocity, yet has a lower normal impact velocity (see Fig. 16). This means that the collisions without the scraper are dominated by tangential interactions and we speculate that they, thus, may not be as efficient in the surface modification as the system with the scraper. It is also possible that the main form of impact occurs from "glancing" collisions with the inner-piece by the particles, which are mostly undergoing rigid body rotation. Further insight into the particle behavior can be obtained by computing the average rotation velocities of the particles, as shown in Fig. 18. Here, it is seen that the particles in the system with the scraper have twice the averaged rotational speed of those without the scraper. However, due to "glancing" collisions taking place in the system without the scraper, the average rotation velocities in the inner-piece region are about the same for both systems.

3.2.4. Frequency and strength of collisions

The results for the average forces and the impact velocities shown in the previous sections indicate the different types of dynamic interactions within the MF

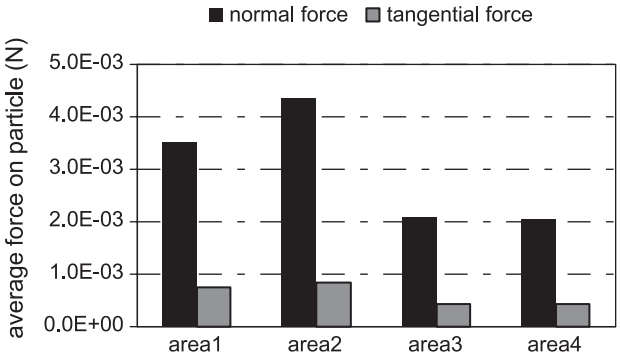

Fig. 15. Average (per particle, per area) normal and tangential impact forces on particles within four different areas as defined in Fig. 14. Also shown are the overall average values.

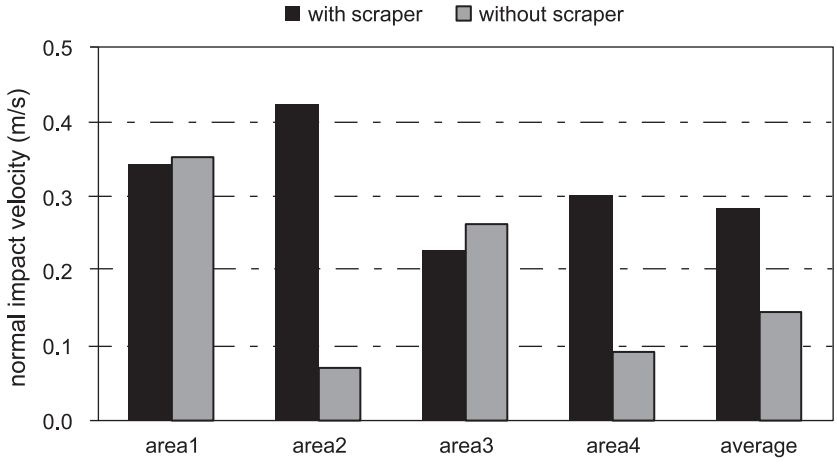

Fig. 16. Average (per particle, per area) normal impact velocities within four different areas as defined in Fig. 14 along with a system average; for system with scraper as well as the system without the scraper.

process. However, in order to use these results in more comprehensive simulations that include guest particle agglomerate break-up and transfer of guest particles from one host to another (guest scale modeling), one needs to know the frequency of the collisions taking place at the device and host scales. For this purpose, the collisions are categorized into collisions that occur between particles and collisions that occur between the particles with the solid boundaries (cylinder boundaries and fixed scraper particles). First, the total number of collisions within each area is calculated, followed by computing the average number of collisions per particle. System parameters for this analysis are also kept the same as in the dynamic analysis presented in the previous section. The total number of collisions is shown in Fig. 19, where in part (a), the collisions with the boundary as a function of time are shown, and in part (b), the collisions between particles as a function of time are shown. As can be seen, the total number of collisions within each area increases linearly with time, as it is a cumulative value. Furthermore, the collisions between the particles and boundary are much smaller in number than the collision between the particles. This is because the projected area in the path of any particle and the other particles is much larger than that of the boundaries.

One counterintuitive observation that can be made is that the total number of collisions in the scraper area is very small as compared to the other zones. On the other hand, the number of collisions within the input area is largest (almost five times that of the scraper area). This discrepancy is explained when the total number of collisions is averaged per particle within a zone, noting that the particle distribution (or packing) is different in different areas. The averaged number of collisions, shown in Fig. 20 is calculated as

$$\text{Averaged collisions} = \frac{\text{cumulative number of collisions within an area}}{\text{average number of particles within the same area}} \quad (12)$$

The plots shown in Fig. 20 provide a clearer picture, as the averaged number of collisions within the free diffusion

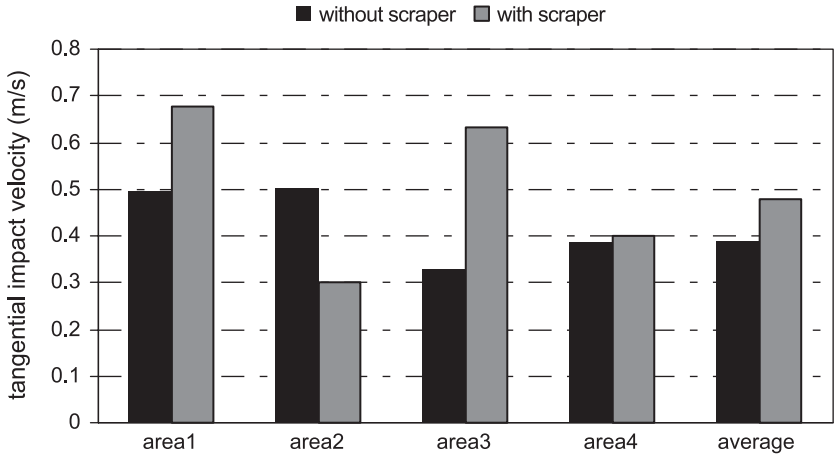

Fig. 17. Average (per particle, per area) tangential impact velocities within four different areas as defined in Fig. 14 along with a system average; for system with scraper as well as the system without the scraper.

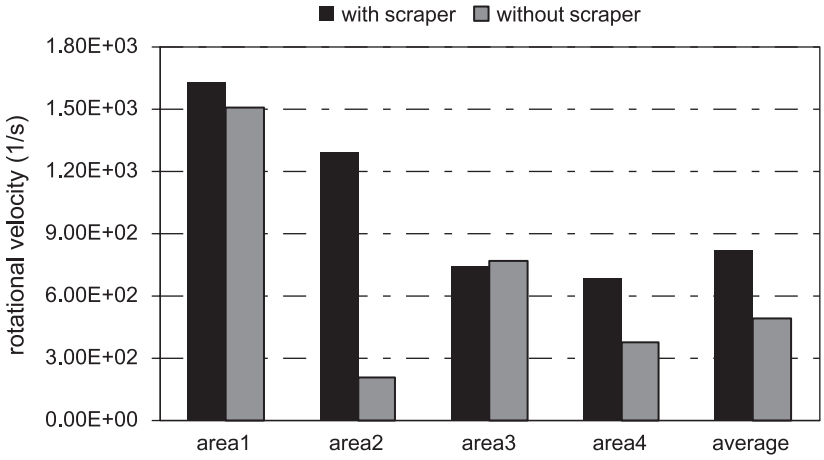

Fig. 18. Average (per particle, per area) rotational velocities within four different areas as defined in Fig. 14 along with a system average; for system with scraper as well as the system without the scraper.

area is smallest, which is also intuitively correct. In this area, a particle has less chance to interact with other particles as well as with the system boundary. On the other hand, the averaged number of collisions within the inner-piece area is the largest, which means that the particles are very active in this area. Also, the averaged number of collisions within the scraper area is smaller compared with the inner-piece area as well as the input area. According to the dynamic analysis in the previous sections, a particle experiences large interaction forces within the scraper area; however, it undergoes lesser interactions with the other elements within this area. Hence, most of the coating action should take place in the inner-piece area when the results of both the collision dynamics and the collision frequency are taken into consideration. The most useful results of the collision analysis are the averaged collision rate in each region. These results, averaged from 3 to 10 s, are shown in Table 2. The values shown in the table are the average number of collisions each particle undergoes in 1 s within different zones, indicating that a single particle may go through tens of thousands of collisions per second.

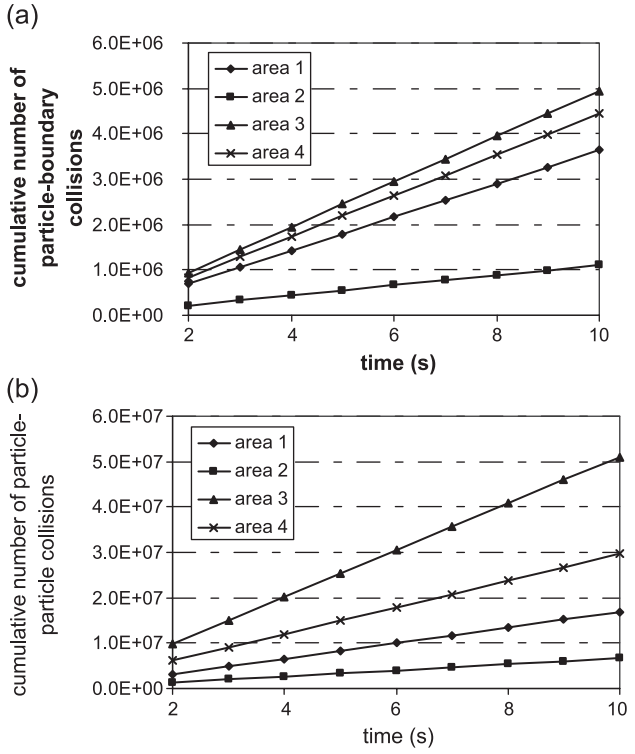

Fig. 19. Cumulative number of collisions within four different areas as defined in Fig. 14; between particles and boundary as well as among particles.

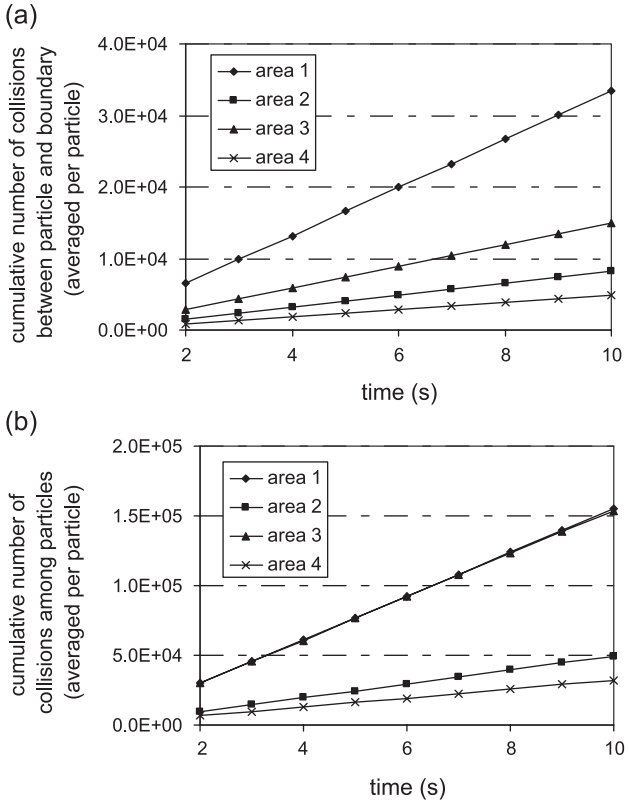

Fig. 20. Cumulative number of collisions per particle within four different areas as defined in Fig. 14; between particles and boundary as well as among particles.

Table 2
Collision frequency within four different areas as defined in Fig. 14 (per particle in 1 s)

	Area 1	Area 2	Area 3	Area 4
Particle–particle	1.54e4	4.92e3	1.52e4	3.14e3
Particle–boundary	3.31e3	8.21e2	1.48e3	4.81e2

Thus it is clear that in the MF system, particle–particle interactions dominate the system behavior.

4. Concluding remarks

In this paper, detailed numerical simulations based on the soft sphere DEM technique are carried out for the Mechanofusion process. The results are part of a long-term project to develop a multi-scale modeling of a dry coating system such as MF, where many different length scales are important. The device and host particle scale simulations performed clearly demonstrated the importance of the scraper to the coating process. Without a scraper, the system exhibits reduced normal impact velocities, indicating that mostly glancing collisions occur between the particles and the inner-piece. Diagnostic analysis of the two systems shows that the numerical simulation can be utilized to visualize the flow pattern and dynamics of the systems, and provide useful insight into the influence of various operating parameters.

Numerical results show that the average force on the inner-piece is a function of the square of the rotational speed of the chamber, in good agreement with experimental results. The simulation is also capable of computing interparticle collision forces between host particles, indicating the strength of the impacts. By calculating average impact forces and average impact velocities for the particles (categorized into four different regions within the system), it is shown that an average particle experiences larger impact forces (or relative impact velocities) in the inner-piece and scraper areas. Based on these results, it seems that the MF system induces collisions that have comparable impact strength in both the normal and tangential directions. These collisions are likely to cause deagglomeration of the fine guest particles so that good coating can take place, particularly (as shown in this paper) since a particle undergoes tens of thousands of collisions per second. It is also shown that while the forces are high in the scraper area, the frequency of collisions is much lower and hence most of the coating activity takes place in the inner-piece region.

It is clear that these type of simulations can be used to derive detailed information about the collision dynamics, including numerical quantities such as relative impact velocities and frequencies of collisions. Future work will focus on utilizing these simulation results combined with the results of guest-scale modeling that will include the break-up of guest particle agglomerates as well as the transfer of guest particles from one host to another in order to develop a more comprehensive modeling of the MF and other dry coating systems.

Acknowledgements

The authors acknowledge financial support for this research from the National Science Foundation under Grant # CTS-9985618 and the New Jersey Commission on Science and Technology under awards # 01-2042-007-24 and # 97-100-020-2890-051-6130.

References

[1] Toh. Yokoyama, K. Urayama, Toy. Yokoyama, KONA 1 (1983) 53.
[2] R. Pfeffer, R. Dave, R.N.D. Wei, M. Ramlakhan, Synthesis of engineered particulates with tailored properties using dry particle coating, Powder Technol. 117 (2001) 40.
[3] Toh. Yokoyama, K. Urayama, Toy. Yokoyama, Kona 5 (1987) 59.
[4] K. Tanno, Kona 8 (1990) 74.
[5] K. Tonno, K. Urayama, T. Yokoyama, R. Watanabe, CIMTEC World Proceedings, Elsevier, 1990.
[6] H. Herman, J. Chen, C. Huang, R. Cohen, Mechanofused powders for thermal spray, J. Therm. Spray Technol. 1 (2) (1992) 129.
[7] J. Chen, C.C. Huang, Kona 15 (1997) 113.
[8] P.A. Cundall, O.D.L. Strack, Geotechnique 29 (1979) 47.
[9] O.R. Walton, R. Braun, J. Rheol. 30 (5) (1986) 949.
[10] O.R. Walton, Mech. Mater. 16 (1993) 239–247.
[11] Y. Tsuji, T. Tanaka, T. Ishida, Powder Technol. 71 (1992) 239.
[12] A.J. Matchett, T. Yanagida, S. Kobayashi, Powder Technol. 107 (n1/2) (2000) 13.
[13] M.P. Allen, D.J. Tildesley, Computer Simulation of Liquids, Clarendon Press, Oxford, 1987.
[14] A. Ladd, Molecular dynamics, Lectures to be Given at the Nato Advanced Summer Institute in Bath, England, 1988, p. 4.
[15] O.R. Walton, in: M.C. Roco (Ed.), Numerical Simulation of Inelastic, Frictional Particle–Particle Interactions, Particulate Two-Phase Flow, Butterworth-Heinemann, 1993, p. 885.
[16] O.R. Walton, J. Appl. Mech. 64 (1997) 247.